~~Impact~~ Numerical simulation of ~~reduced emissions~~ the impact of COVID-19 lockdown on ~~direct~~ tropospheric composition and ~~indirect~~ aerosol radiative forcing ~~during COVID–19 lockdown~~ in Europe

Simon F. Reifenberg[1,a], Anna Martin[1], Matthias Kohl[1], Zaneta Hamryszczak[1], Ivan Tadic[1], Lenard Röder[1], Daniel J. Crowley[1], Horst Fischer[1], Katharina Kaiser[2], Johannes Schneider[2], Raphael Dörich[1], John N. Crowley[1], Laura Tomsche[3], Andreas Marsing[3], Christiane Voigt[3,4], Andreas Zahn[5], Christopher Pöhlker[6], Bruna A. Holanda[6], Ovid Krüger[6], Ulrich Pöschl[6], Mira Pöhlker[6,7,8], Patrick Jöckel[3], Marcel Dorf[1], Ulrich Schumann[3], Jonathan Williams[1], Joachim Curtius[9], Hardwig Harder[1], Hans Schlager[3], Jos Lelieveld[1,10], and Andrea Pozzer[1,10]

[1]Max Planck Institute for Chemistry, Atmospheric Chemistry Department, 55128 Mainz, Germany
[2]Max Planck Institute for Chemistry, Particle Chemistry Department, 55128 Mainz, Germany
[3]Deutsches Zentrum für Luft– und Raumfahrt, Institute for Atmospheric Physics, Oberpfaffenhofen, 82230 Wessling, Germany
[4]Johannes Gutenberg–University Mainz, Institute for Physics of the Atmosphere, 55099 Mainz, Germany
[5]Institute of Meteorology and Climate Research, Karlsruhe Institute of Technology, 76344 Karlsruhe, Germany
[6]Max Planck Institute for Chemistry, Multiphase Chemistry Department, 55128 Mainz, Germany
[7]Faculty of Physics and Earth Sciences, Leipzig Institute for Meteorology, University of Leipzig, 04318 Leipzig, Germany
[8]Experimental Aerosol and Cloud Microphysics Department, Leibniz Institute for Tropospheric Research,04318 Leipzig, Germany
[9]Goethe–University of Frankfurt, Institute for Atmospheric and Environmental Sciences, 60438 Frankfurt am Main, Germany
[10]The Cyprus Institute, Climate and Atmosphere Research Center, Nicosia, 1645, Cyprus
[a]now at: MARUM – Center for Marine Environmental Science, University of Bremen, Bremen, Germany

Correspondence: Andrea Pozzer (andrea.pozzer@mpic.de)

Abstract.

Aerosols influence the Earth's energy balance ~~through direct radiative effects~~ directly by modifying the radiation transfer and indirectly by altering the cloud microphysics. Anthropogenic aerosol emissions dropped considerably when the global ~~COVID–19~~ COVID-19 pandemic resulted in severe restraints on mobility, production, and public life in spring 2020. ~~Here we~~ We assess the effects of these reduced emissions on direct and indirect aerosol radiative forcing over Europe, excluding contributions from contrails. We simulate the atmospheric composition with the ECHAM5/MESSy Atmospheric Chemistry (EMAC) model in a baseline (business as usual) and a reduced emission scenario. The model results are compared to aircraft observations from the BLUESKY aircraft campaign performed in May/June 2020 over Europe. The model agrees well with most of the observations, except for sulfur dioxide, particulate sulfate and nitrate in the upper troposphere, likely due to a ~~somewhat~~ biased representation of stratospheric aerosol chemistry and missing information about volcanic eruptions~~which could have influenced the campaign~~. The comparison with a ~~business as usual~~ baseline scenario shows that the largest relative differences for tracers and aerosols are found in the upper troposphere, around the aircraft cruise altitude, due to the reduced aircraft emissions, while the largest absolute changes are present at the surface. We also find an increase in all sky shortwave radiation of ~~0.327 ± 0.105~~ 0.21 ± 0.05 $\mathrm{W m^{-2}}$ at the surface in Europe for May 2020, solely attributable to the direct aerosol effect, which is dominated by decreased aerosol scattering of sunlight, followed by reduced aerosol absorption, caused by lower concentrations of inorganic and black carbon aerosols in the troposphere. A further increase in shortwave radiation from aerosol indirect effects was found to be much smaller than its variability. Impacts on ice ~~crystal- and~~ crystal concentrations, cloud droplet number concentrations, and effective crystal radii are found to be negligible.

1 Introduction

Aerosols play a pivotal role in both air pollution and climate change. They ~~cause millions of years of lost life expectancy per year globally~~ have large impact on human health (Lelieveld et al., 2015, 2020), impose a negative (net) effective radiative forcing (Bellouin et al., 2020), and are a large source of uncertainty in climate change assessments. A reduction of the cooling effect by a decreased aerosol burden necessitates stronger reductions of greenhouse gases (GHGs) for a targeted net radiative forcing ~~(Larson and Portmann, 2019)~~(Larson and Portmann, 2019; Myhre et al., 2013).

Owing to the central importance of aerosol particles, the reduced emissions resulting from drastic restrictions on mobility, industry and public life during the ~~COVID–19~~ COVID-19 "lockdowns" in early 2020 (~~here~~ hereafter referred to as "lockdown") (Barré et al., 2020; Evangeliou et al., 2021; Guevara et al., 2021; Le Quéré et al., 2020) sparked a plethora of publications on the subsequent effects on local, regional, and global air pollution (see, for instance, He et al., 2020; Liu et al., 2020; Petetin et al., 2020; Tobías et al., 2020; Venter et al., 2020; Mertens et al., 2021)~~and climatic effects, on which we will focus in this work~~.

We recognise that reduced emissions during lockdown do not necessarily translate into improved air quality, as primary pollutants take part in a complex set of chemical processes, which need to be included in a thorough analysis (Kroll et al., 2020). For instance, although ozone was reported to be reduced in the free troposphere in the northern hemisphere (Steinbrecht et al., 2021), the reduced emissions of the nitrogen oxides NO and NO_2 led to an increase in ozone concentrations in urban locations, as an important short-term sink (reaction with NO) was reduced (e.g. Gkatzelis et al., 2021; Sicard et al., 2020; Mertens et al., 2021). This illustrates how the complex (photo-)chemistry and the nonlinearity of the underlying chemical system have to be described and analyzed within the framework of a dynamic atmospheric chemistry model. A chemistry climate model with appropriate chemistry furthermore enables a direct comparison of ~~business as usual~~ baseline and reduced emissions within the same synoptic background conditions, complementary to a purely observation-based approach. ~~Such model investigations are most effective when accompanied and guided by observational data, as will be done in the present study~~Many works are present in the literature that investigate the climatic effect of COVID-19 lockdown (e.g. Lee et al., 2021; Forster et al., 2020; Gettelman et al., 2021). Of particular importance is the CovidMIP intercomparison project, where 12 global chemistry climate model were used to investigate the impact of COVID-19 lockdown on the radiation (Jones et al., 2021; Lamboll et al., 2021), with special focus on aerosol-radiation interaction.

The interaction of aerosols with radiation and their climatic impact can be categorized into two types: (i) direct effects by impact on radiation fluxes, and (ii) indirect effects through changes in cloud physical and optical properties.

The direct effects include absorption and scattering of electromagnetic waves, whereby aerosol particles, most prominently black carbon (BC), absorb incoming solar radiation, which leads to warming of the ambient air and decreases solar irradiance in the layers below. In addition, aerosols scatter incident radiation back to space, leading to a net cooling of the climate system on average. These processes depend on the size, shape and chemical composition of the aerosols and on the wavelength of the radiation. In addition, the net effect depends on the surface albedo ~~(Yoon et al., 2019; Bellouin et al., 2020).~~

(Shindell et al., 2013; Yoon et al., 2019; Bellouin et al., 2020). The reduced emissions in spring 2020 are thus expected to affect aerosol radiative forcing. A reduction in the backscattering of solar radiation is expected to result in warming, which is offset by the anticipated cooling effect through a reduction of black carbon emissions, and the net effect may vary vertically and horizontally. For instance, Gettelman et al. (2021) reported a simulated net warming at the surface and in the lower troposphere in most regions, caused by enhanced insolation at the surface, and cooling in upper layers of the troposphere, due to reduced absorption by black carbon. They also determined a difference in the clear sky net shortwave (SW) flux at the top of the atmosphere (TOA) of up to $0.1\ \mathrm{Wm^{-2}}$ globally in May 2020 between simulations with and without reduced emissions, i.e. less outgoing SW radiation due to the lockdown. Complementing the analyses regarding these more immediate effects, Forster et al. (2020) estimate a short-term warming driven by a weakened aerosol cooling through reduced sulfur dioxide ($\mathrm{SO_2}$) emissions, followed by a cooling of $0.010 \pm 0.005\ \mathrm{K}$ by 2030 in reference to a baseline scenario.

~~Tracks of conducted flights during the BLUESKY campaign (16th May to 9th June 2020). Colors denote the aircraft, Falcon (blue) and HALO (red).~~

In addition to the aerosol direct effects on the radiation budget, aerosol particles ~~can trigger~~ have several indirect effects. Aerosol particles serve as cloud condensation nuclei and thus can potentially alter cloud properties, such as cloud albedo, cloud droplet number concentration, formation processes, precipitation and cloud lifetime (see, for instance, Bellouin et al., 2020; Christensen et al., 2020; Lohmann and Feichter, 2005; Twomey, 1959). In turn, clouds also affect aerosols. Clouds convert precursor gases into aerosol particles through heterogeneous chemistry (Ervens et al., 2011; Lelieveld and Heintzenberg, 1992; McMurry and Wilson, 1983) and, at the same time, remove aerosols and soluble gases from the atmosphere by precipitation ("wet deposition").

~~Clouds are classified based on their liquid water or ice content, since these characteristics determine the efficiency of reflection of solar radiation back to space (cloud albedo effect) and the absorption rate of longwave radiation (greenhouse effect), thus their impact on the Earth's radiation budget. Clouds consisting only of ice crystals (e.g. cirrus clouds) occur mostly in high altitudes at temperatures below the homogeneous freezing threshold of~~ $\sim -35^\circ\mathrm{C}$ ~~(Pruppacher and Klett, 1997; Kärcher and Seifert,~~

~~. Ice crystals (ICs) are formed either due to homogeneous or heterogeneous freezing depending on aerosol characteristics and number concentration, temperature, supersaturation and vertical air motion (Pruppacher and Klett, 1997). IC number densities in cirrus clouds are typically lower (Voigt et al., 2017) compared to clouds at lower altitude, and cirrus clouds are often optically thin and transmit shortwave radiation and absorb longwave radiation, resulting in an overall positive net radiative effect at the TOA (Bacer et al., 2018, 2021; Gasparini et al., 2017). In contrast, mixed-phase clouds, consisting of ICs and cloud droplets,~~

~~form only due to heterogeneous nucleation at lower altitudes and temperatures higher than -35°C. These optically thick clouds reflect a comparably large amount of the incoming SW radiation, leading to a negative net radiative effect at the TOA (Chen et al., 2000). The cloud albedo effect can be enhanced by the Twomey effect (Twomey, 1959), whereby high number concentrations of CCN lead to a higher number of droplets of smaller size compared to clouds formed with lower number of CCN. Accordingly, clouds, containing more droplets of smaller sizes, reflect solar radiation more strongly than clouds containing fewer droplets of larger size. This effect is especially important over the ocean, where the number of natural CCNs, compared to anthropogenic CCNs, is much lower than over land (Lohmann and Feichter, 2005). Ship emissions, including aerosol particles, create clouds with a much higher reflectivity (or albedo) than clouds formed by the less numerous natural CCNs outside of the ship tracks (Platnick et al., 2000). The same effect arises in aircraft flight tracks, where the emitted particles may act as ice nucleating particles, leading to contrail formation (Schumann et al., 2017) and an increase in cirrus cloud formation in the upper troposphere (Boucher, 1999). Still, the magnitude of the aviation soot effect on the radiation budget remains uncertain (Urbanek et al., 2018; Righi et al., 2021)~~Radiative forcing from aerosol cloud interactions is very challenging to quantify, and it is strongly model dependent (Hong et al., 2016; Gasparini and Lohmann, 2016; Myhre et al., 2013) . Recently, satellite data have been used to quantify changes in clouds in regions with COVID-reduced airtraffic in 2020 (Quaas et al., 2021; Gettelman et al., 2021). With respect to contrails, Schumann et al. (2021a, b) find a substantial reduction of contrail cirrus optical thickness and radiative forcing during the lockdown period.

~~The modification of cloud cover resulting from differing particle number concentrations has further effects on the lifetime of a cloud. An increase in smaller cloud particles makes the clouds more persistent and delays the occurrence of precipitation (referred to as cloud lifetime effect, Lohmann and Feichter, 2005). Increased cloud lifetime affects not only the timing but also the location of precipitation. The increased lifetime of clouds also extends the period over which a cloud can reflect radiation, thus adding to the Twomey effect. With increasing aerosol number concentration corresponding to a negative perturbation of the radiation budget, both effects contribute to cooling~~ Complex model as the one used by the CovidMIP, however, are most effective when accompanied by observational data, as the capability of the models to reproduce the real atmosphere is unclear, especially when the anthropogenic emissions are strongly perturbed as in the case of the COVID-19 lockdown. Furthermore, as the reduced emissions have different effect on the atmospheric composition depending also on the altitude, the observational data should cover large regions of the troposphere. Despite the large presence of observations at the surface ~~and at the TOA (Lohmann and Feichter, 2005). The number and size distribution of cloud nucleating particles can thus affect the extent of transmission of radiation~~during the COVID-19 lockdown (Gkatzelis et al., 2021), the free and upper troposphere presented comparably almost none in situ measurements against which the model could be validated. One notable exception is the BLUESKY field campaign (Voigt et al., 2021); from 16th May to 9th June 2020 in situ measurements of trace gases and trace particles were conducted in the atmosphere over European urban areas and the North Atlantic flight corridor with the High Altitude and Long Range (HALO) research aircraft and a second research aircraft, Falcon (see Fig. 1 for flight paths). Comprehensive measurements of trace gases and aerosols composition were conducted, providing a unique set of observations that can be used to validate model results.

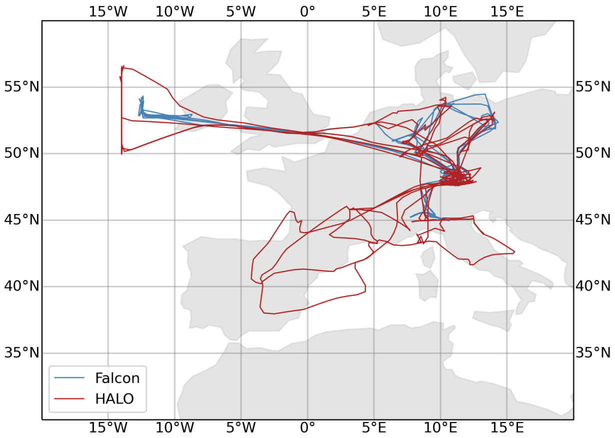

Figure 1. Tracks of conducted flights during the BLUESKY campaign (16th May to 9th June 2020). Colors denote the aircraft, Falcon (blue) and HALO (red).

Using an observation-guided model, the ~~COVID–19~~ COVID-19 lockdown provided an opportunity to examine how the climate system reacts to perturbations such as abruptly reduced air pollution emissions. The ~~COVID–19~~ COVID-19 lockdown may also serve to assess the impact of economic recovery with respect to climate change mitigation: for instance, Forster et al. (2020) show that investments aimed at a "green" opposed to a fossil-fueled recovery can reduce projected warming by 0.3 K by 2050, with only negligible contributions from the lockdown.

In the present study, we simulate the chemical composition of the atmosphere in Europe in spring 2020 under a reduced emission scenario and a ~~business as usual~~ baseline scenario with a state-of-the-art climate and chemistry simulation system, constraining atmospheric dynamics by reanalysis meteorological data. We use ~~a unique~~ the BLUESKY observational data set of trace gases and aerosols obtained during an aircraft measurement campaign in Europe during the ~~COVID–19~~ COVID-19 lockdown in summer 2020 to evaluate the model results. We then quantify the effects of the lockdown on radiative transfer in the atmosphere, particularly the change in shortwave fluxes and shortwave heating rates attributable to a reduced aerosol burden in Europe. Furthermore, we examine the impacts of the ~~lockdown scenario~~ reduced emissions on cloud properties, including potential changes of the radiative forcing caused by indirect aerosol effects.

~~This paper is structured as follows. In Sect. 2 we describe the model together with an overview of the simulations performed (Sect. 2.1), as well as the observational data (Sect. 2.2). The model evaluation is presented in Sect. 3. We then investigate the impacts of the reduced emissions during the 2020 COVID–19 lockdown on direct aerosol effects and indirect cloud–aerosol effects (Sect. 4).~~

2 Data and methods

2.1 Model data

The ECHAM5/MESSy Atmospheric Chemistry (EMAC) model is a numerical chemistry and climate simulation system that includes submodels describing tropospheric and middle atmospheric processes and their interaction with oceans, land and human influences (Jöckel et al., 2016). It uses the second version of the Modular Earth Submodel System (MESSy2) to link multi-institutional computer codes. The core atmospheric model is the 5th generation European Centre Hamburg general circulation model (ECHAM5, Roeckner et al., 2006).

For the present study we applied EMAC (ECHAM5 version 5.3.02, MESSy version 2.55.0) in T63L47MA-resolution, i.e. with a spherical truncation of T63 (corresponding to a quadratic Gaussian grid of approx. 1.8 by 1.8 degrees in latitude and longitude) with 47 vertical hybrid pressure levels up to 1 Pa. Roughly 22 levels are included in the troposphere, and the model has a time step of 300 seconds. The dynamics of the EMAC model has been weakly nudged ~~(Jeuken et al., 1996; Jöckel et al., 2006) towards the ERA–interim~~ in the troposphere (Jeuken et al., 1996; Jöckel et al., 2006; Jeuken et al., 1996; Löffler et al., 2016) towards the ERA5 meteorological reanalysis data ~~(Berrisford et al., 2011)~~ (Hersbach et al., 2020) of the European Centre for Medium-Range Weather Forecasts (ECMWF) to represent the actual day to day meteorology in the troposphere.

The setup of the chemistry submodels for this study is similar to the one presented by Jöckel et al. (2016, simulation RC1–aero–07), but with the addition of the submodel ORACLE (Tsimpidi et al., 2014) for the organic chemistry calculation and with stratospheric heterogeneous chemistry neglected. Initial conditions for the meteorology were also taken from the ERA–interim reanalysis data, while the ones for the chemical composition were from previous EMAC simulations (Pozzer et al., 2022). In addition, the anthropogenic emissions used are based on CAMS–GLOB–ANTv4.2 (Granier et al., 2019). To reproduce the effect of lockdown on the emissions, we adopted the reduction coefficient for Europe as in Guevara et al. (2021) for the sectors of energy production (ENE), road transport (TRO) and industrial processes (IND). The reduced emissions were averaged for the period 19th April to 26th of April (i.e. last available week in the dataset), and applied (for each country) for March, April, May and June. For aviation (AVI) we adopted the same method, although we applied the estimated factor to the entire aviation emissions, without any country distinction.

~~The aerosol–cloud interactions are based on the aerosol microphysics parameterization of Pringle et al. (2010) including aerosol aging and the continuous calculation of aerosol number concentration depending on the~~ Atmospheric aerosols are described via a two-moment aerosol scheme, which predicts number concentration and mass mixing ratio ~~and mixing state. Additionally, cloud formation~~ of the aerosol modes (Pringle et al., 2010). This scheme takes into account various physical-chemical processes of aerosols, such as coagulation, aging, condensation, and also the gas—aerosol partitioning (Fountoukis and Nenes, 2007). Convective cloud processes are accounted for using the ~~convection~~ framework of Tost et al. (2006), based on the convection ~~calculation~~ schemes of Tiedtke (1989) and Nordeng (1994). ~~Large-scale cloud formations and prognostic variables depending on cloud microphysical processes follow the work of Lohmann et al. (2007); Lohmann and Hoose (2009); Bacer et al. (2018). Thereby, the~~ Convective cloud microphysics does not take into account the influence of aerosols on liquid droplet or ice formation processes and is solely based on temperature and vertical velocity. In EMAC, the vertical velocity is given by the sum of the grid mean vertical velocity and the turbulent contribution (Brinkop and Roeckner, 1995), thus one single updraught velocity is used for the whole grid cell. Large-scale stratiform clouds are described by the CLOUD submodel, which, in the setup applied here, uses a two-moment cloud microphysics scheme for cloud droplets and ice crystals (Lohmann et al., 1999; Lohmann and . and solves the prognostic equations for specific humidity, liquid cloud mixing ratio, ice cloud mixing ratio, cloud droplet number concentration (CDNC), and ice crystal number concentration (ICNC). The model setup without cloud-aerosol interactions uses the original ECHAM5 cloud microphysical scheme (Lohmann and Roeckner, 1996) and a statistical cloud cover scheme including prognostic equations for the distribution moments (Sundqvist et al., 1989). Details on the cloud microphysical scheme can be found in Roeckner et al. (2003, and references therein).

Cloud droplet formation in the model setup without cloud-aerosol interaction is computed by the “unified activation framework”, an advanced physically based parameterization (Kumar et al., 2009; Karydis et al., 2011) that combines the κ-Köher theory (Petters and Kreidenweis, 2007) for the activation of soluble aerosols with the Frenkel–Halsey–Hill adsorption activation theory (Kumar et al., 2009) for the droplet activation due to water adsorption onto insoluble aerosols. Ice formation occurs via homogeneous ice nucleation following the parameterization of Barahona and Nenes (2009) and heterogeneous ice nucleation of insoluble dust, insoluble black carbon, and glassy organics following Phillips et al. (2013). In the cirrus regime (~~$T \leq 238.15$)~~$T \leq 238.15K$), the effect of pre-existing ice crystals and the competition for the available water vapor between homogeneous and heterogeneous ice nucleation mechanisms are taken into account (Bacer et al., 2018). Given the high contribution of instantaneous freezing (Bacer et al., 2021), the ICNC in the cirrus regime was modified according to Neubauer et al. (2019) in order to reduce the artificial homogeneous freezing of dry aerosol particles independent of availability of water vapor. Other microphysical processes related to cloud droplets and ice crystals, like phase transitions, autoconversion, aggregation, accretion, evaporation, melting, are also taken into account by the CLOUD submodel. The cloud cover is computed diagnostically with the scheme of Sundqvist et al. (1989), which is based on the grid-mean relative humidity.

The aerosol forcing of the EMAC model has been investigated, and here we report the Effective radiative forcing of the aerosol radiation interaction (ERF$_{\mathrm{ari}}$) and the Effective radiative forcing of the aerosol cloud interaction (ERF$_{\mathrm{aci}}$), based on the definition of Myhre et al. (2013). Following the work of Lelieveld et al. (2019), the EMAC model in a setup very similar to ours, simulates a radiative forcing global mean of all anthropogenic aerosols at TOA (top of the atmosphere) of $-0.46 \pm 0.01 W m^{-2}$ and $-1.2 \pm 0.1 W m^{-2}$ for ERF$_{\mathrm{ari}}$ and ERF$_{\mathrm{ari}}$+ERF$_{\mathrm{aci}}$, respectively. At BOA (bottom of the atmosphere) the model simulates $-1.6 \pm 0.02 W/m^{-2}$ and $-2.1 \pm 0.1 W/m^{-2}$ for ERF$_{\mathrm{ari}}$ and ERF$_{\mathrm{ari}}$+ERF$_{\mathrm{aci}}$, respectively.

We performed four simulations, all covering the period from January 2019 to July 2020:

- ~~STD~~ BASE : standard (i.e. "~~business as usual~~baseline") emissions, without cloud–aerosol interaction,
- RED : reduced emissions due to lockdown, without cloud–aerosol interaction,
- ~~STDCLOUD : like STD~~ BASECLOUD : like BASE but with aerosol–cloud interaction,
- REDCLOUD : like RED but with aerosol–cloud interaction.

In all simulations performed, the impact of different aerosol concentrations on the radiation (discussed in Sect. 4.2.1) is diagnosed but not used by the general circulation model, which instead adopts an aerosol climatology (Pringle et al., 2010). Similarly, changes in the tracers (e.g. ozone) do not influence the radiation, which is calculated with a greenhouse gases climatology.

The model evaluation is performed with the RED simulation, while its difference with the ~~STD~~ BASE simulation is used to evaluate the impact of the reduced emissions during the lockdown. Simulation RED and ~~STD~~ BASE have binary identical dynamics (Deckert et al., 2011), i.e. they reproduce numerically exactly the same dynamics, as no feedback between chemistry and dynamic is present. Differently, in REDCLOUD and ~~STDCLOUD~~BASECLOUD, the aerosol–cloud interaction is activated following the work of Lohmann and Hoose (2009); Bacer et al. (2018), leading to modification of cloud properties and therefore to changes in radiation and dynamics. The simulations REDCLOUD and ~~STDCLOUD~~ BASECLOUD are only used for estimating the indirect effects of aerosols (see Sect. 4.2.2).

2.2 BLUESKY observational data

We compare simulated trace gas and aerosol abundances to a comprehensive set of observations obtained during the BLUESKY campaign (Voigt et al., 2021)~~, led by the German Aerospace Center (DLR) and the Max Planck Institute for Chemistry (MPIC), with the aim of investigating the effects of reduced emissions on atmospheric chemistry and physics. From 16th May to 9th June 2020 in~~. In situ measurements of trace gases and trace particles were conducted end of May 2022 in the atmosphere over ~~European urban areas and the North Atlantic flight corridor with the High Altitude and Long Range (HALO) research aircraft and a second research aircraft, Falcon (see Fig. 1 for flight paths)~~Europe with the Falcon and HALO research aircraft. In total 8 and 12 flights were conducted with the HALO and the Falcon, respectively (Fig. 1).

We compare aerosol mass concentrations of black carbon (BC, size range between 70 and 500 nm), sulfate (SO_4^{2-}), nitrate (NO_3^-), ammonium (NH_4^+), organic aerosol particles (ORG, all from 40 to 800 nm) and aerosol particle number concentrations (between 250 nm to 40 µm). These are complemented by volume mixing ratios of carbon monoxide (CO), ozone (O_3), nitric oxide (NO), hydrogen peroxide (H_2O_2), peroxyacetyl nitrate (PAN), nitric acid (HNO_3), and sulfur dioxide (SO_2). Details regarding instrumentation are provided by Voigt et al. (2021). We additionally use air temperature T, wind speed and specific humidity q to assess the quality of the reproduced synoptic conditions which are constrained (nudged) in the model. For the comparison, the model output was sampled ~~online in space and time~~ during runtime by the submodel S4D (Jöckel et al., 2016), following the flight tracks of the field campaign and with a time frequency of 5 minutes.

3 ~~Results:~~ Model evaluation

~~A summary of the comparison of observations and model results is listed in and presented graphically in Figs. 2 and 3.~~

The ambient air temperature T is reproduced very well by the model; the average ratio of observed and simulated T is equal to 1.00 with a normalized root mean squared error of 0.04 (NRMSE; RMSE divided by range of observations). The vertical temperature profile is matched in the lower and free troposphere with a slight underestimation of observed temperatures towards the upper troposphere (Fig. 2), which confirms the quality of the nudged data. Specific humidity q, a quantity that is not subject to nudging, is also captured reasonably well in the model, (NRMSE = 0.06), as 85.9 % of simulated values lie within a factor of two of the observations, yet slightly overestimated (see Fig. 2 and Table 1). In addition, horizontal wind speed $||\boldsymbol{u}_h||$ is also reproduced accurately with a low NRMSE (0.06) and an average ratio of 1.02.

Overall, the agreement between the meteorological variables from model and ~~observations~~ the one observed in the BLUESKY campaign indicates successful initialization and nudging of meteorological variables and that the meteorological conditions during the relevant time period are simulated adequately. As the model is not nudged in the stratosphere or boundary layer (the nudging coefficient is maximal in the free troposphere (Jöckel et al., 2006)), the ~~slight underestimation of temperature~~ deviation in the upper troposphere ~~region is not surprising~~between model results and observational data are to be expected, due to the intrinsic model dynamics which deviates from the nudging data. Nevertheless, the temperature bias is much lower than in other EMAC studies, despite the use of same nudging method and coefficients (Jöckel et al., 2016), due to the intialization and shorter simulation time in this work. As temperature and humidity are important quantities regarding cloud formation, and accurate wind vectors are key for representing advective processes, the following analyses of atmospheric composition and the effects on radiative transfer build on an accurate representation of the meteorological state of the model.

3.1 Trace gases

~~Observed~~ More than 94 % of simulated ozone (O_3) mixing ratios are ~~reproduced well by the model. More than 94 % of simulated values are~~ within a factor of 2 of the observations ("PF2" value) ~~,~~ and the normalized root mean squared error of 0.04 is low, with improvements from previous evaluation of the same model (Jöckel et al., 2016). Nevertheless, the model seems to slightly overestimate the observations, as already pointed out in various studies (e.g. Jöckel et al., 2016).

Simulated carbon monoxide (CO) mixing ratios are also in a good agreement with the observations, and virtually all simulated values lie within a factor of two of the observations. However, especially at lower altitudes, the simulated mixing ratios ~~somewhat~~ underestimate the observed values, although the difference between average observations and average model results are well within their respective variability, and the shape of the vertical profile is qualitatively well reproduced. The same holds for nitric oxide (NO), which exhibits a C-shaped profile. The NRMSE for NO is low (0.08) and the average ratio of simulated to observed mixing ratio is 0.99, however more than a third of simulated values deviate more than a factor of two from the observations, due to the high variability of this tracer. Particularly the range of the observed mixing ratios close to the surface is not well reproduced by the model, which results from the short lifetime of NO and the challenge in reproducing its local variation by a global model.

Hydrogen peroxide (H_2O_2) and peroxyacetyl nitrate (PAN) are less well represented, the average ratios of simulated to observed mixing ratio (2.01 for H_2O_2 and 1.91 for PAN) indicate an overestimation by the model. Nevertheless, for both species about two thirds of the simulated points are still within a factor of two of the observations (see Fig. 2), and the measured dependence on altitude is captured by the model.

Sulfur dioxide (SO_2) was sampled predominantly at high altitudes between 370 to 170 hPa, where it is strongly underestimated by the model. We hypothesize that the systematic underestimation of SO_2 concentrations is due to ~~an inaccurate~~

Table 1. Summary of model–observations comparison. The same spatio-temporal location were used for all simultaneously available points . NRMSE shows the root mean squared error normalized by the range of the observations. PF2 denotes the percentage of model points within a factor of 2 of the observations. The column $\overline{\text{MOD/OBS}}$ is the average of the simulated and observed data ratios.

Variable	NRMSE	PF2	$\overline{\text{MOD/OBS}}$
Trace gases			
O_3	0.04	94.7	1.25
CO	0.14	99.3	0.98
NO	0.08	65.0	0.99
H_2O_2	0.32	61.5	2.01
PAN	0.13	60.3	1.91
HNO_3	0.37	12.9	0.46
SO_2	0.40	25.9	0.43
Aerosols			
BC	0.09	18.6	0.68
NO_3^-	0.14	20.6	0.92
NH_4^+	0.22	28.8	0.83
SO_4^{2-}	0.16	26.8	0.72
Organics	0.45	40.6	1.73
Number conc.	0.11	42.8	2.60
Meteorology			
T	0.04	100.0	1.00
q	0.06	85.9	1.27
$\|\|\boldsymbol{u}_h\|\|$	0.06	100.0	1.02

~~representation of transport from the boundary layer or from the stratosphere to the upper troposphere or due to~~ model shortcomings within the stratospheric aerosol chemistry, which will be discussed briefly as part of the following Sect. 3.2. All in all, as summarized in Table 1, there is reasonable agreement between observed and simulated mixing ratios of the trace gases investigated.

3.2 Aerosols

In the comparison between model results and aerosol observations, the instrumental cut-offs have been taken into account; the aerosol log-normal modes in the model have been integrated only in the appropriate range, so to have a reasonable comparison. In addition, all the measurements and model results are based on location pressure and temperature and are not normalized to Standard Temperature and Pressure (STP).

The vertical profile of the measured aerosol number concentration is qualitatively reproduced (see Fig. 3~~)~~, with logarithmic scale in the x-axis), with a minimum at $\simeq 300$ hPa and a maximum at the surface. In the lowest altitude pressure bin, the range and median of the observations and model results match very well. There are some deviations between 850 and 480 hPa, where simulated number concentrations are larger than the observed ones, although this overestimation is well within the observations' variability. This overestimation dominates the average ratio of modeled to measured values (2.60, see Table 1).

The measured black carbon (BC) concentrations are captured well by the model close to the surface, while the observational variability is underestimated at high altitudes. The NRMSE of 0.09 is relatively low, as the higher abundance closer to the surface – that is, closer to the sources – is well represented, both in terms of magnitude and variability. A detail analysis of the black carbon concentration simulated with the EMAC model during the BLUESKy campaign can be found in Krüger et al. (2022).

Sulfate (SO_4^{2-}) exhibits qualitatively similar features as BC; the relatively high concentrations observed in the lower troposphere are matched by the simulated concentrations, yet there is a significant underestimation of sulfate aerosol concentrations in the upper troposphere. ~~We hypothesize that the modeled underestimation of sulfur species is related to missing contribution of volcanic eruptions that have reached the stratosphere at low latitudes and return to the troposphere at higher latitude. Many small and medium size eruptions have been reported in the year prior to the BLUESKY campaign (, last access 30. October 2021), but their influence on the upper troposphere and lower stratosphere is yet to be quantified. Some preliminary test simulations are mentioned below.~~

Between 1050 and 625 hPa simulated organic aerosol concentrations are somewhat larger in the model than in reality, the shape of the vertical profile is, however, qualitatively reproduced.

Nitrate (NO_3^-) and ammonium (NH_4^+) concentrations close to the surface are generally well reproduced. While, at higher altitudes, the simulated NH_4^+ agrees with the observations, simulated nitrate is too high, which is probably related to the co-located underestimation of sulfate.

The results of the model/measurement comparison are summarised in Table 1. We ~~conclude~~ can observe that there is generally reasonable agreement between simulated and observed trace gases and aerosols with some deviation of the aerosol concentrations, especially in the mid-upper troposphere.

A single ~~factor~~ emissions source causing the model underestimation of BC and sulfate aerosol concentrations in the upper troposphere, e.g. a localized plume of pollution, is judged unlikely, as BC and SO_4^{2-} do not correlate ($r < 0.01$, $p = 0.90$): in fact, mapping observed SO_4^{2-} concentrations to ozone (a tracer of stratospheric air), and carbon monoxide (a tracer of tropospheric air), reveals that high SO_4^{2-} concentrations coincide with high ozone ($r = 0.83$, $p < 0.01$) and low carbon monoxide ($r = -0.65$, $p < 0.01$) (Fig. 4). A similar, yet weaker, correspondence can be found in the simulated data (see Fig. 4). ~~This suggests~~ The strong correlation with ozone in the upper troposphere implies a stratospheric source of sulfate aerosols in both model and reality~~, although stratospheric sulfate aerosol appears to be represented poorly in the model~~. It is noteworthy that a precursor for sulfate aerosols, sulfur dioxide, is also systematically underestimated. We assume hence that the high SO_2 abundance measured ~~is of volcanic origin~~in the upper troposphere has stratospheric origin and is from volcanic eruptions. Many small and medium size eruptions have been reported in the year prior to the BLUESKY campaign (https://volcano.si.edu, last access 30. October 2021), but their influence on the upper troposphere and lower stratosphere is yet to be quantified. We tested this by injecting high levels of SO_2 in the stratosphere in additional simulations, mimicking volcanic eruptions ~~at~~ that had enough energy to reach the stratosphere, i.e. Raikoke (June) and Ulawun (June and August) in 2019 (see de Leeuw et al., 2021; Kloss et al., 2021). However, this did not affect the concentrations of SO_4^{2-} and NO_3^- significantly (not shown). A partial increase of SO_4^{2-} was obtained by including the volcanic eruption of Taal in January 2020. Nevertheless this is still not enough to bring the model results close to the observations. We therefore conclude that our observed underestimation of SO_4^{2-} is of stratospheric origin, although it is not fully clear what caused it.

A further partition of the region of interest into three subregions (Central Europe, Southern Europe, Atlantic) did not reveal substantial spatial dependencies of model deviation from observations (not shown).

4 ~~Results:~~ Impact of reduced emissions

To quantify the effect of the lockdown, we use the ~~business as usual simulations (STD and STDCLOUD~~baseline simulations (BASE and BASECLOUD) in the analyses. We focus on May 2020, as this time period is covered by the measurement campaign and the atmosphere can be expected to have adjusted to the impact of abruptly reduced emissions. We also analyse the impact in an area encompassing Europe (the region of study), i.e. over a longitude-latitude box from -20 to 20° E and 30 to 60° N (exactly the depicted map sector in Fig. 1).

4.1 Impact on tracers and aerosols

~~As no feedback between chemistry and dynamics is activated in the RED and STD simulations , any~~ As no difference in dynamics between RED and BASE simulations are present, any chemical differences between these simulations are purely attributable to the different emissions during the lockdown period, as these are the only changes between these two simulations, and the consequent different chemical regimes.

In general, while large absolute changes are expected at the surface, in the upper troposphere (UT) we find the largest relative changes, due to the strong influence of the local emissions and to the low mixing ratios of most of the species investigated (see Fig. 5). Large relative changes in the UT are found for NO, SO_2 and BC, with a strong reduction (~ 50 % or more) in the region between 200 and 300 hPa, i.e. the typical aircraft cruise altitude. The reduced air traffic during the lockdown period greatly decreased the emissions of nitrogen oxides into the UT, and the effects of the lockdown on other tracers in the UT are mostly a result of this strong reduction. Hydroxyl radicals (OH) decrease by roughly 20 % in the UT and 5 % elsewhere in the troposphere, a direct effect of a reduced OH recycling by NO_x. Despite the reduced OH, carbon monoxide does not increase, due to the decrease in the direct emissions. The overall effect of the lockdown for most ~~tracer~~ tracers is a combination of reduced emissions and reduced sinks (i.e. oxidation via OH): while this is well balanced for CO (changes in the order of few percent), for SO_2 the emission reductions are larger than the decrease in the reaction with OH, causing its mixing ratio to be reduced (up to 50 % in the UT) compared to the ~~business as usual scenario. It must be stressed however, that those relative changes in the upper troposphere, although significant, have a very minor impact on most trace gas budgets, due to their low mixing ratios at these altitudes.~~ baseline scenario.

Similar to the trace gases, for most aerosols the lockdown reduces their concentration mostly at the surface, although the largest relative differences are simulated in the UT, due to the low concentration at these altitudes. For example, sulfate is subject to a large relative change in the UT but to much larger absolute changes close to the surface, mimicking the changes in SO_2 (see also Fig. 6). Furthermore, BC decreases significantly in the whole troposphere, due to the strong reduction of the emissions both at the surface and in the UT (from aircraft). ~~The aerosol reductions during the lockdown have implications on the incoming shortwave radiation, as discussed in the next section~~

While the changes in CO and NO can be considered significant and representative of the real atmospheric changes (due to the low bias at all tropospheric levels between model results and observations), changes in the aerosol components should be considered with caution, as these are generally smaller than the bias between the model results and the observations.

4.2 Impact on shortwave radiation

As the model is nudged in the troposphere (i.e. constrained air temperature with prescribed sea surface temperatures) ~~, we do not investigate any effects on the outgoing longwave radiation.Rather, we~~ and free to adjust dynamics of the stratosphere, we report here RF (radiative forcing) values (Myhre et al., 2013). For the same reason (i.e. tropospheric nuding), we mostly focus the analyses on the shortwave flux F_{SW} and its induced heating rate $(\partial T/\partial t)_{\mathrm{SW}}$ in the area encompassing Europe, as these are directly influenced by the aerosols changes and are not strongly influenced by the numerical forcing.

4.2.1 Direct effects

Aerosols directly impact the radiation balance by absorption and scattering of electromagnetic waves. Compared to the ~~business as usual~~ baseline emissions, the monthly mean sulfate (and inorganic aerosols, not shown) and black carbon concentrations are reduced ~~most strongly close to the surface, with another (much smaller) local maximum close to~~ in all troposphere, with a strong relative reduction at the commercial flight level (around 200 hPa, see ~~also~~ Fig. 6). Furthermore, the mean aerosol (number) concentrations were reduced in the ~~lockdown scenario~~ scenario with reduced emissions due to lockdown throughout the whole air column (see Fig. 8 and Sect. 4.2.2), with the reduction being most pronounced between 300 and 200 hPa~~, likely~~ . Based on model results from a sensitivity simulation, where only the aircraft emissions where reduced compared to the BASE simulation, we estimated that more than 90% of the reduced aerosols number between 300 and 200 hPa over Europe is due to reduced aircraft emissions~~and the effect on particle formation and coagulation at these altitudes~~.

We calculate the simulated difference in the downwelling shortwave flux between simulation RED and STD, i.e. the impact of the reduced emissions on the SW radiation. Here only the aerosol contribution is estimated, removing any radiative effect from changes in trace gases (e.g. ozone) within the Europe longitude-latitude box for May 2020. The differences are largest over continental central Europe and lowest over Northern Scandinavia (Fig. 7), with no large spatial gradients over Europe. In virtually all regions there is more downwelling shortwave radiation in the reduced emission scenario. Spatially averaged at ground level within the European domain, there is an increase of ~~0.327 ± 0.105~~ 0.33 ± 0.10 $\mathrm{Wm^{-2}}$ under clear sky condition (i.e., no clouds) compared to the baseline scenario, while at the TOA the increase is ~~0.198 ± 0.092~~ 0.20 ± 0.09 $\mathrm{Wm^{-2}}$. This increase, together with the reduced heating rates of ambient air, is indicative of a reduction in shortwave scattering and absorption, due to the reduced inorganic aerosol and black carbon concentrations, i.e. the lockdown contributed to make the atmosphere more transparent to SW radiation. ~~We also compared our results with Van Heerwaarden et al. (2021): our radiative effect of all aerosols in our RED simulation for May is of -3.33 ± 1.36 , which is close to their value of -2.3 .~~The column integrated contribution of backscatter and absorption can be estimated from the radiation values at TOA and surface, indicating that, during lockdown, the total backscatter (clear sky) of SW radiation has been decreased by ~~0.263 ± 0.070~~ 0.26 ± 0.07 Wm^{-2}, while the total absorption (clear sky) was decreased by ~~0.064 ± 0.053~~ 0.06 ± 0.05 Wm^{-2}. Based on an additional sensitivity simulations, in which only individual emissions (i.e. of BC, SO_2, ~~with~~ NO) have been reduced, we found that slightly more than one third of ~~this~~ the absorption reduction is caused by the BC decrease.

Reduced scattering by aerosol particles plays a larger role, as the "net" (i.e. the difference attributable to the lockdown) shortwave flux is positive in the whole air column; on the other hand, reduced absorption dominates the shortwave component of direct aerosol effects in the boundary layer, as clearly shown in Fig. 6. The heating of ambient air exhibits a local minimum in the upper troposphere, which is however small compared to that in the lower troposphere. We calculate the surface integral of the accumulated heating due to shortwave fluxes, only attributable to aerosols under clear sky conditions: the difference in the atmospheric layer directly above the surface is -0.005 ± 0.001 $\mathrm{K/day}$, i.e. less heating of the boundary layer in the lockdown conditions compared to normal emissions. ~~The decreased heating (for the entire column but mostly at the surface) is due~~ Based on a sensitivity simulation similar to RED but without any reduction in BC, we found that the decreased heating is by 40% to the reduced absorption by BC during the lockdown conditions, causing a cooling of the atmosphere (through SW radiation) despite an increase of the incoming radiation. Both the changes in heating and shortwave flux are solely attributable to the different aerosol burden in the ~~STD~~ BASE and RED simulations.

We also estimated also the $\mathrm{RF_{ari}}$ Myhre et al. (2013) due to COVID-19 lockdown against the baseline scenario, by including also the longwave radiation. We obtained an $\mathrm{RF_{ari}}$ equal to 0.08 ± 0.03 for all sky over Europe in May 2020 at the TOA. This value, although accounting only for a limited amount of the anthropogenic aerosols (the lockdown did not removed all anthropogenic emissions) and referring only for Europe, is within the range suggested by Bellouin et al. (2020, ,see Tab.5).

4.2.2 Aerosol–cloud interactions

In Fig. 8, the vertical distributions of the total aerosol number concentration (N, including all aerosol sizes), ice crystal number concentration (ICNC), cloud droplet number concentration (CDNC) and ice crystal radius (r) are shown for Europe for both simulations, ~~STDCLOUD~~ BASECLOUD and REDCLOUD. Additionally, the SW flux at the TOA and the surface have been calculated from these coupled aerosol–cloud simulations (see Table 2), both for the total effect (i.e. direct plus indirect) and for the indirect (i.e. neglecting any direct radiation influence of the aerosol particles). Due to the short simulation period, the difference between these simulations is much smaller than its variability, represented by its spatial and temporal standard deviation. Nevertheless, comparing the vertical distribution of number concentrations of aerosols, ice crystals and cloud droplets, the largest relative difference between ~~STDCLOUD~~ BASECLOUD and REDCLOUD (i.e. the two simulations where the aerosol–cloud feedback is activated) is found for the aerosol number concentration between 200 and 300 hPa. These are the cruise altitudes at which the largest aircraft emissions are injected in the model and therefore these differences can be directly connected to the reduced air traffic present during the lockdown (REDCLOUD). As this altitude is somewhat higher than the typical (cold) cloud altitude, the effect on clouds is less pronounced. At the highest level of these clouds (see Fig. 8) the ICNC are reduced (by $\simeq 30$ % at 250 hPa, although with large variability), while no visible effect is found for CDNC. These results are in line with those obtained by Righi et al. (2021), who showed that aircraft emissions do increase ice crystal number concentration, although their results were not statistically significant. The ice crystal effective radius seems to be the least affected by the reduced emissions during the ~~COVID–19~~ COVID-19 lockdown, with a negligible absolute and relative difference.

To investigate the effect of reduced aircraft emissions on the SW flux via the indirect aerosol effect at the TOA and surface (SRF), the mean differences in SW flux between REDCLOUD and ~~STDCLOUD~~ BASECLOUD for May were calculated over Europe. Positive values indicate greater reflection of SW radiation back to space (for TOA) or more absorption through the troposphere (for surface values) in the ~~STDCLOUD~~ BASECLOUD simulation, compared to the REDCLOUD. The mean surface differences are ~~0.307 ± 0.115~~ 0.31 ± 0.11 $\mathrm{Wm^{-2}}$ for the clear sky and ~~0.443 ± 1.063~~ 0.44 ± 1.06 $\mathrm{Wm^{-2}}$ for the all sky case. At the TOA the mean differences in shortwave fluxes are ~~0.186 ± 0.106~~ 0.19 ± 0.11 $\mathrm{Wm^{-2}}$ (clear sky) and ~~0.281 ± 0.928~~ 0.28 ± 0.93 $\mathrm{Wm^{-2}}$ (all sky, Table 2). We should ~~notice~~ note that the clear sky results agree with the direct effect estimated in Sect.4.2.1 but with different simulations, confirming the consistency of the calculations. Thus, the indirect effect of aerosols enhances the direct effect on the SW radiation during the lockdown, even with larger intensity. ~~This confirms the importance of the cloud–aerosol interaction, as mentioned by Hong et al. (2016), Gasparini and Lohmann (2016) and Myhre et al. (2013) .~~ However, those values are associated with large standard deviations, related to the strong spatial variability of the upward shortwave radiation difference between the simulations.

The total $\mathrm{RF_{aci}}$ due to COVID-19 lockdown against the baseline scenario was also estimated. We obtained a value of 0.19 ± 0.92 for all sky over Europe in May 2020 at the TOA. Similarly to $\mathrm{RF_{ari}}$, also this value is in line with the range suggested by Bellouin et al. (2020, ,see Tab.5), keeping in mind that only a partial reduction of anthropogenic aerosols took place during the COVID-19 lockdown. Although the average value agree with the literature, a large standard deviation is associated to $\mathrm{RF_{aci}}$, so that the estimate should be taken with caution as not statistical significant.

5 Conclusions

We simulated the effects of drastically reduced anthropogenic emissions on the atmospheric composition in Europe during the ~~COVID–19~~ COVID-19 lockdown in spring 2020. We evaluated the model simulations with observations obtained during the aircraft measurement campaign BLUESKY. The overall agreement between observations and simulated aerosol concentrations and trace gas mixing ratios is reasonable. Nevertheless, problems remain regarding stratosphere–troposphere transport, especially of volcanic influence, which resulted in systematically underestimated SO_2 and SO_4^{2-} of stratospheric origin, and a consequent overestimation of NO_3^- ~~(which substitutes the underestimated sulfate in ammonium salts)~~ (which substitutes the underestimated su
in the upper troposphere.

Table 2. Aerosol direct and indirect effects on the shortwave radiation flux at the top of atmosphere (TOA) and surface (SRF) over Europe for May compared to baseline scenario. Note that direct effects are derived from ~~STD~~ BASE and RED simulations, and indirect and total (i.e. direct plus indirect) effects from ~~STDCLOUD~~ BASECLOUD and REDCLOUD. The indirect effect of clear sky estimation is obviously equal to zero, but it was included to confirm the validity of the calculations.

	RED−~~STD~~ BASE	REDCLOUD−BASECLOUD	
ΔF_{SW} $[\mathrm{Wm^{-2}}]$	direct	indirect	total
TOA	~~0.090 ± 0.035~~ 0.09 ± 0.03	~~0.188 ± 0.759~~ 0.19 ± 0.76	~~0.281 ± 0.928~~ 0.28 ± 0.93
TOA clear sky	~~0.198 ± 0.092~~ 0.20 ± 0.09	~~0.000 ± 0.006~~ 0.00 ± 0.01	~~0.186 ± 0.106~~ 0.19 ± 0.11
SRF	~~0.209 ± 0.053~~ 0.21 ± 0.05	~~0.233 ± 1.089~~ 0.23 ± 1.09	~~0.443 ± 1.063~~ 0.44 ± 1.06
SRF clear sky	~~0.327 ± 0.105~~ 0.33 ± 0.10	~~0.001 ± 0.023~~ 0.00 ± 0.02	~~0.307 ± 0.115~~ 0.31 ± 0.11

Focusing on the effects of aerosol particles on the shortwave radiation budget, we find that their reduction due to lockdown leads to a net clear sky SW flux increase of ~~0.327 ± 0.105 and 0.198 ± 0.092~~ 0.33 ± 0.10 and 0.20 ± 0.09 $\mathrm{Wm^{-2}}$ at surface level and TOA over Europe, respectively. The increase of the SW radiation during the lockdown period is due to the decrease of both black carbon and inorganic aerosols, which made the atmosphere more transparent to the incoming solar radiation by reducing SW absorption and SW backscatter, with the latter dominating. It must be stressed that although this BC reduction causes an increase in the SW incoming radiation, the SW heating has also been reduced by up to $0.005\ \mathrm{K/day}$, due to the lowered BC absorption.

With reduced emissions, the model simulates a lower number concentration of aerosols between 300 and 50 hPa; this reduction is located at an altitude too high to ~~effectively influence the cold cirrus clouds (aircraft cruising altitude, ≃ 250 hPa)~~influence the cloud droplet formation (Karydis et al., 2017) and heterogeneous ice nucleation from black carbon and dust; glassy organics freeze at these altitudes, but their contribution is totally negligible in comparison with homogeneous nucleation (Bacer et al., 2021). The analysis of the indirect aerosol effect did not give any conclusive results, due to the large variability in the calculations caused by the short duration of the lockdown "experiment".

Note that contrails and their contribution to radiative forcing are not considered in this study. Contrails are expected to reduce solar radiation reaching the Earth surface and to reduce outgoing longwave radiation. The mean changes induced by reduced air traffic in 2020 compared to 2019, computed in two model studies, were of the order of -0.1 to $0.5\ \mathrm{Wm^{-2}}$ over Europe (Gettelman et al., 2021; Schumann et al., 2021b), ~~so at~~ with a magnitude comparable to ~~the aerosol effects~~ what found in this study. ~~We therefore plan to include contrail effects in a forthcoming study~~ The differences between these studies, can partly be attributed to the applied methodologies and general difficulties in discriminating anthropogenic effects from interannual variability. Hence, a study which considers contrail and aerosol effects simultaneously, and covers a longer time period, is recommended to better attribute the causes of the observed changes .

Code availability. The Modular Earth Submodel System (MESSy) is continuously further developed and applied by a consortium of institutions. The usage of MESSy and access to the source code is licensed to all affiliates of institutions which are members of the MESSy Consortium. Institutions can become a member of the MESSy Consortium by signing the MESSy Memorandum of Understanding. More information can be found on the MESSy Consortium Website (http://www.messy-interface.org). The code presented here has been based on MESSy version 2.55 and is available as git commit #dcdc3ed8, in the MESSy repository.

Data availability. The observational data and the model results are available on the HALO (High Altitude Long RAnge research aircraft) database (https://halo-db.pa.op.dlr.de), upon sign of data protocol.

Author contributions. A.P. and S.R. planned the research. A.P. and S.R. collected and prepared the emission data. A.M. implemented code corrections for aerosol-cloud interactions. A.P. performed the model simulations. P.J. contributed to the overall model development and helped with the preparation of the model setups. M.K. provided the script for the aerosol mass estimation in the model. Z.H., I.T., L.R., D.J.C. and H.F. provided the data for CO, NO and $\mathrm{H_2O_2}$. J.S. and K.K. provided observational aerosol composition data. R.D. and J.N.C. were responsible for the PAN measurements. C.V., L.T. and A.M. provided observational data of $\mathrm{HNO_3}$ and $\mathrm{SO_2}$. A.Z. provided the ozone data. O.K., B.H., C.P., M.P. and U.P. were conducting, analyzing and interpreting the BC data. M.D. organized the field campaign logistically. J.C. planned the flight tracks during the campaign. H.S. coordinated the measurements on the FALCON. S.R. and A.P. performed the model evaluation and analysis of direct effects. A.M. and A.P. performed the analysis of indirect effects. U.S. and A.P. discussed the results on the radiative forcing. S.R., A.M and A.P. wrote the manuscript with the help of J.C., M.K. and J.W.. A.P. and J.L. supervised the project. All authors discussed the results and contributed to the review and editing of the manuscript.

Competing interests. The authors declare that they have no conflict of interest.

Acknowledgements. Christiane Voigt, Laura Tomsche and Andreas Marsing thank funding by the HGF and by the DFG within the SPP1294 HALO under contract no Vo1504/7-1 and the TRR301-1 TP change.

References

Bacer, S., Sullivan, S. C., Karydis, V. A., Barahona, D., Krämer, M., Nenes, A., Tost, H., Tsimpidi, A. P., Lelieveld, J., and Pozzer, A.: Implementation of a comprehensive ice crystal formation parameterization for cirrus and mixed-phase clouds in the EMAC model (based on MESSy 2.53), Geoscientific Model Development, 11, 4021–4041, 2018.

Bacer, S., Sullivan, S. C., Sourdeval, O., Tost, H., Lelieveld, J., and Pozzer, A.: Cold cloud microphysical process rates in a global chemistry–climate model, Atmospheric Chemistry and Physics, 21, 1485–1505, https://doi.org/10.5194/acp-21-1485-2021, 2021.

Barahona, D. and Nenes, A.: Parameterizing the competition between homogeneous and heterogeneous freezing in ice cloud formation–polydisperse ice nuclei, Atmospheric Chemistry and Physics, 9, 5933–5948, 2009.

Barré, J., Petetin, H., Colette, A., Guevara, M., Peuch, V.-H., Rouil, L., Engelen, R., Inness, A., Flemming, J., Pérez García-Pando, C., Bowdalo, D., Meleux, F., Geels, C., Christensen, J. H., Gauss, M., Benedictow, A., Tsyro, S., Friese, E., Struzewska, J., Kaminski, J. W., Douros, J., Timmermans, R., Robertson, L., Adani, M., Jorba, O., Joly, M., and Kouznetsov, R.: Estimating lockdown induced European NO_2 changes, Atmospheric Chemistry and Physics Discussions, 2020, 1–28, https://doi.org/10.5194/acp-2020-995, in review, 2020.

Bauer, S. E., Koch, D., Unger, N., Metzger, S. M., Shindell, D. T., and Streets, D. G.: Nitrate aerosols today and in 2030: a global simulation including aerosols and tropospheric ozone, Atmospheric Chemistry and Physics, 7, 5043–5059, https://doi.org/10.5194/acp-7-5043-2007, 2007.

Bellouin, N., Quaas, J., Gryspeerdt, E., Kinne, S., Stier, P., Watson-Parris, D., Boucher, O., Carslaw, K. S., Christensen, M., Daniau, A.-L., Dufresne, J.-L., Feingold, G., Fiedler, S., Forster, P., Gettelman, A., Haywood, J. M., Lohmann, U., Malavelle, F., Mauritsen, T., McCoy, D. T., Myhre, G., Mülmenstädt, J., Neubauer, D., Possner, A., Rugenstein, M., Sato, Y., Schulz, M., Schwartz, S. E., Sourdeval, O., Storelvmo, T., Toll, V., Winker, D., and Stevens, B.: Bounding Global Aerosol Radiative Forcing of Climate Change, Reviews of Geophysics, 58, e2019RG000 660, https://doi.org/10.1029/2019RG000660, e2019RG000660 10.1029/2019RG000660, 2020.

Berrisford, P., Dee, D., Poli, P., Brugge, R., Fielding, M., Fuentes, M., Kållberg, P., Kobayashi, S., Uppala, S., and Simmons, A.: The ERA–Interim archive Version 2.0, p. 23, https://www.ecmwf.int/node/8174, 2011.

Boucher, O.: Air traffic may increase cirrus cloudiness, Nature, 397, 30–31, https://doi.org/10.1038/16169, number: 6714 Publisher: Nature Publishing Group, 1999.

Brinkop, S. and Roeckner, E.: Sensitivity of a general circulation model to parameterizations of cloud–turbulence interactions in the atmospheric boundary layer, Tellus A, 47, 197–220, 1995.

Chen, T., Rossow, W. B., and Zhang, Y.: Radiative Effects of Cloud–Type Variations, Journal of Climate, 13, 264–286, https://doi.org/10.1175/1520-0442(2000)013<0264:REOCTV>2.0.CO;2, publisher: American Meteorological Society Section: Journal of Climate, 2000.

Christensen, M. W., Jones, W. K., and Stier, P.: Aerosols enhance cloud lifetime and brightness along the stratus-to-cumulus transition, Proceedings of the National Academy of Sciences, 117, 17 591–17 598, https://doi.org/10.1073/pnas.1921231117, 2020.

de Leeuw, J., Schmidt, A., Witham, C. S., Theys, N., Taylor, I. A., Grainger, R. G., Pope, R. J., Haywood, J., Osborne, M., and Kristiansen, N. I.: The 2019 Raikoke volcanic eruption – Part 1: Dispersion model simulations and satellite retrievals of volcanic sulfur dioxide, Atmospheric Chemistry and Physics, 21, 10 851–10 879, https://doi.org/10.5194/acp-21-10851-2021, 2021.

Deckert, R., Jöckel, P., Grewe, V., Gottschaldt, K.-D., and Hoor, P.: A quasi chemistry-transport model mode for EMAC, Geoscientific Model Development, 4, 195–206, 2011.

Ervens, B., Turpin, B. J., and Weber, R. J.: Secondary organic aerosol formation in cloud droplets and aqueous particles (aqSOA): a review of laboratory, field and model studies, Atmospheric Chemistry and Physics, 11, 11 069–11 102, https://doi.org/10.5194/acp-11-11069-2011, 2011.

Evangeliou, N., Platt, S. M., Eckhardt, S., Lund Myhre, C., Laj, P., Alados-Arboledas, L., Backman, J., Brem, B. T., Fiebig, M., Flentje, H., Marinoni, A., Pandolfi, M., Yus-Dìez, J., Prats, N., Putaud, J. P., Sellegri, K., Sorribas, M., Eleftheriadis, K., Vratolis, S., Wiedensohler, A., and Stohl, A.: Changes in black carbon emissions over Europe due to COVID–19 lockdowns, Atmospheric Chemistry and Physics, 21, 2675–2692, https://doi.org/10.5194/acp-21-2675-2021, 2021.

Forster, P. M., Forster, H. I., Evans, M. J., Gidden, M. J., Jones, C. D., Keller, C. A., Lamboll, R. D., Quéré, C. L., Rogelj, J., Rosen, D., Schleussner, C.-F., Richardson, T. B., Smith, C. J., and Turnock, S. T.: Current and future global climate impacts resulting from COVID–19, Nature Climate Change, 10, 913–919, https://doi.org/10.1038/s41558-020-0883-0, 2020.

Fountoukis, C. and Nenes, A.: ISORROPIA II: a computationally efficient thermodynamic equilibrium model for K+–Ca 2+–Mg 2+–NH 4+–Na+–SO 4 2—NO 3—Cl—H 2 O aerosols, Atmospheric Chemistry and Physics, 7, 4639–4659, 2007.

Gasparini, B. and Lohmann, U.: Why cirrus cloud seeding cannot substantially cool the planet, Journal of Geophysical Research: Atmospheres, 121, 4877–4893, 2016.

Gasparini, B., Münch, S., Poncet, L., Feldmann, M., and Lohmann, U.: Is increasing ice crystal sedimentation velocity in geoengineering simulations a good proxy for cirrus cloud seeding?, Atmospheric Chemistry and Physics, 17, 4871–4885, https://doi.org/10.5194/acp-17-4871-2017, 2017.

Gettelman, A., Lamboll, R., Bardeen, C. G., Forster, P. M., and Watson-Parris, D.: Climate Impacts of COVID–19 Induced Emission Changes, Geophysical Research Letters, 48, e2020GL091 805, https://doi.org/10.1029/2020GL091805, e2020GL091805 2020GL091805, 2021.

Gkatzelis, G. I., Gilman, J. B., Brown, S. S., Eskes, H., Gomes, A. R., Lange, A. C., McDonald, B. C., Peischl, J., Petzold, A., Thompson, C. R., and Kiendler-Scharr, A.: The global impacts of COVID–19 lockdowns on urban air pollution: A critical review and recommendations, Elementa: Science of the Anthropocene, 9, https://doi.org/10.1525/elementa.2021.00176, 00176, 2021.

Granier, C., Darras, S., Denier van der Gon, H., Doubalova, J., Elguindi, N., Galle, B., Gauss, M., Guevara, M., Jalkanen, J.-P., Kuenen, J., Liousse, C., Quack, B., Simpson, D., and Sindelarova, K.: The Copernicus Atmosphere Monitoring Service global and regional emissions (April 2019 version), Copernicus Atmosphere Monitoring Service (CAMS) report, https://doi.org/10.24380/d0bn-kx16, 2019.

Guevara, M., Jorba, O., Soret, A., Petetin, H., Bowdalo, D., Serradell, K., Tena, C., Denier van der Gon, H., Kuenen, J., Peuch, V.-H., and Pérez García-Pando, C.: Time-resolved emission reductions for atmospheric chemistry modelling in Europe during the COVID–19 lockdowns, Atmospheric Chemistry and Physics, 21, 773–797, https://doi.org/10.5194/acp-21-773-2021, 2021.

He, G., Pan, Y., and Tanaka, T.: The short-term impacts of COVID–19 lockdown on urban air pollution in China, Nature Sustainability, 3, 1005–1011, https://doi.org/10.1038/s41893-020-0581-y, 2020.

Hersbach, H., Bell, B., Berrisford, P., Hirahara, S., Horányi, A., Muñoz-Sabater, J., Nicolas, J., Peubey, C., Radu, R., Schepers, D., et al.: The ERA5 global reanalysis, Quarterly Journal of the Royal Meteorological Society, 146, 1999–2049, 2020.

Hong, Y., Liu, G., and Li, J.-L.: Assessing the radiative effects of global ice clouds based on CloudSat and CALIPSO measurements, Journal of Climate, 29, 7651–7674, 2016.

Jeuken, A., Siegmund, P., Heijboer, L., Feichter, J., and Bengtsson, L.: On the potential of assimilating meteorological analyses in a global climate model for the purpose of model validation, Journal of Geophysical Research: Atmospheres, 101, 16 939–16 950, 1996.

Jöckel, P., Tost, H., Pozzer, A., Brühl, C., Bucholz, J., L., G., Hoor, P., Kerkweg, A., Lawrence, M., Sander, R., Steil, B., Stiller, G., Tanarhte, M., Taraborrelli, D., van Aardenne, J., and Lelieveld, J.: Evaluation of the atmospheric chemistry GCM ECHAM5/MESSy: Consistent simulation of ozone in the stratosphere and troposphere, Atmos. Chem. Phys., 6, 5067–5104, 2006.

Jöckel, P., Tost, H., Pozzer, A., Kunze, M., Kirner, O., Brenninkmeijer, C. A. M., Brinkop, S., Cai, D. S., Dyroff, C., Eckstein, J., Frank, F., Garny, H., Gottschaldt, K.-D., Graf, P., Grewe, V., Kerkweg, A., Kern, B., Matthes, S., Mertens, M., Meul, S., Neumaier, M., Nützel, M., Oberländer-Hayn, S., Ruhnke, R., Runde, T., Sander, R., Scharffe, D., and Zahn, A.: Earth System Chemistry integrated Modelling (ESCiMo) with the Modular Earth Submodel System (MESSy) version 2.51, Geoscientific Model Development, 9, 1153–1200, https://doi.org/10.5194/gmd-9-1153-2016, 2016.

Jones, C. D., Hickman, J. E., Rumbold, S. T., Walton, J., Lamboll, R. D., Skeie, R. B., Fiedler, S., Forster, P. M., Rogelj, J., Abe, M., et al.: The climate response to emissions reductions due to COVID-19: Initial results from CovidMIP, Geophysical research letters, 48, e2020GL091 883, 2021.

Kärcher, B. and Seifert, A.: On homogeneous ice formation in liquid clouds, Quarterly Journal of the Royal Meteorological Society, 142, 1320–1334, 2016.

Karydis, V., Kumar, P., Barahona, D., Sokolik, I., and Nenes, A.: On the effect of dust particles on global cloud condensation nuclei and cloud droplet number, Journal of Geophysical Research: Atmospheres, 116, 2011.

Karydis, V. A., Tsimpidi, A. P., Bacer, S., Pozzer, A., Nenes, A., and Lelieveld, J.: Global impact of mineral dust on cloud droplet number concentration, Atmospheric Chemistry and Physics, 17, 5601–5621, 2017.

Kloss, C., Berthet, G., Sellitto, P., Ploeger, F., Taha, G., Tidiga, M., Eremenko, M., Bossolasco, A., Jégou, F., Renard, J.-B., and Legras, B.: Stratospheric aerosol layer perturbation caused by the 2019 Raikoke and Ulawun eruptions and their radiative forcing, Atmospheric Chemistry and Physics, 21, 535–560, https://doi.org/10.5194/acp-21-535-2021, 2021.

Kroll, J. H., Heald, C. L., Cappa, C. D., Farmer, D. K., Fry, J. L., Murphy, J. G., and Steiner, A. L.: The complex chemical effects of COVID–19 shutdowns on air quality, Nature Sustainability, 12, 777–779, https://doi.org/10.1038/s41557-020-0535-z, 2020.

Krüger, O. O., Holanda, B. A., Chowdhury, S., Pozzer, A., Walter, D., Pöhlker, C., Andrés Hernández, M. D., Burrows, J. P., Voigt, C., Lelieveld, J., Quaas, J., Pöschl, U., and Pöhlker, M. L.: Black carbon aerosol reductions during COVID-19 confinement quantified by aircraft measurements over Europe, Atmospheric Chemistry and Physics Discussions, 2022, 1–36, https://doi.org/10.5194/acp-2021-1100, 2022.

Kumar, P., Sokolik, I., and Nenes, A.: Parameterization of cloud droplet formation for global and regional models: including adsorption activation from insoluble CCN, Atmospheric Chemistry and Physics, 9, 2517–2532, 2009.

Lamboll, R. D., Jones, C. D., Skeie, R. B., Fiedler, S., Samset, B. H., Gillett, N. P., Rogelj, J., and Forster, P. M.: Modifying emissions scenario projections to account for the effects of COVID-19: protocol for CovidMIP, Geoscientific Model Development, 14, 3683–3695, 2021.

Larson, E. J. L. and Portmann, R. W.: Anthropogenic aerosol drives uncertainty in future climate mitigation efforts, Scientific Reports, 9, 16 538, https://doi.org/10.1038/s41598-019-52901-3, 2019.

Le Quéré, C., Jackson, R. B., Jones, M. W., Smith, A. J. P., Abernethy, S., Andrew, R. M., De-Gol, Anthony J. Willis, D. R., Shan, Y., Canadell, J. G., Friedlingstein, P., Creutzig, F., and Peters, G. P.: Temporary reduction in daily global CO 2 emissions during the COVID–19 forced confinement, Nature Climate Change, 10, 647–653, https://doi.org/10.1038/s41558-020-0797-x, 2020.

Lee, S.-S., Chu, J.-E., Timmermann, A., Chung, E.-S., and Lee, J.-Y.: East Asian climate response to COVID-19 lockdown measures in China, Scientific reports, 11, 1–9, 2021.

Lelieveld, J. and Heintzenberg, J.: Sulfate cooling effect on climate through in-cloud oxidation of anthropogenic SO2, Science, 258, 117–120, 1992.

Lelieveld, J., Evans, J. S., Fnais, M., Giannadaki, D., and Pozzer, A.: The contribution of outdoor air pollution sources to premature mortality on a global scale, Nature, 525, 367–371, https://doi.org/10.1038/nature15371, 2015.

Lelieveld, J., Klingmüller, K., Pozzer, A., Burnett, R. T., Haines, A., and Ramanathan, V.: Effects of fossil fuel and total anthropogenic emission removal on public health and climate, Proceedings of the National Academy of Sciences, 116, 7192–7197, https://doi.org/10.1073/pnas.1819989116, 2019.

Lelieveld, J., Pozzer, A., Pöschl, U., Fnais, M., Haines, A., and Münzel, T.: Loss of life expectancy from air pollution compared to other risk factors: a worldwide perspective, Cardiovascular Research, 116, 1910–1917, https://doi.org/10.1093/cvr/cvaa025, 2020.

Liu, F., Page, A., Strode, S. A., Yoshida, Y., Choi, S., Zheng, B., Lamsal, L. N., Li, C., Krotkov, N. A., Eskes, H., van der A, R., Veefkind, P., Levelt, P. F., Hauser, O. P., and Joiner, J.: Abrupt decline in tropospheric nitrogen dioxide over China after the outbreak of COVID–19, Science Advances, 6, https://doi.org/10.1126/sciadv.abc2992, 2020.

Löffler, M., Brinkop, S., and Jöckel, P.: Impact of major volcanic eruptions on stratospheric water vapour, Atmospheric Chemistry and Physics, 16, 6547–6562, https://doi.org/10.5194/acp-16-6547-2016, 2016.

Lohmann, U. and Feichter, J.: Global indirect aerosol effects: a review, Atmospheric Chemistry and Physics, 5, 715–737, https://doi.org/10.5194/acp-5-715-2005, publisher: Copernicus GmbH, 2005.

Lohmann, U. and Hoose, C.: Sensitivity studies of different aerosol indirect effects in mixed-phase clouds, Atmospheric Chemistry and Physics, 9, 8917–8934, 2009.

Lohmann, U. and Kärcher, B.: First interactive simulations of cirrus clouds formed by homogeneous freezing in the ECHAM general circulation model, Journal of Geophysical Research: Atmospheres, 107, AAC–8, 2002.

Lohmann, U. and Roeckner, E.: Design and performance of a new cloud microphysics scheme developed for the ECHAM general circulation model, Climate Dynamics, 12, 557–572, 1996.

Lohmann, U., Feichter, J., Chuang, C. C., and Penner, J. E.: Prediction of the number of cloud droplets in the ECHAM GCM, Journal of Geophysical Research: Atmospheres, 104, 9169–9198, 1999.

Lohmann, U., Stier, P., Hoose, C., Ferrachat, S., Kloster, S., Roeckner, E., and Zhang, J.: Cloud microphysics and aerosol indirect effects in the global climate model ECHAM5–HAM, Atmos. Chem. Phys., p. 22, 2007.

McMurry, P. H. and Wilson, J. C.: Droplet phase (Heterogeneous) and gas phase (homogeneous) contributions to secondary ambient aerosol formation as functions of relative humidity, Journal of Geophysical Research: Oceans, 88, 5101–5108, https://doi.org/https://doi.org/10.1029/JC088iC09p05101, 1983.

Mertens, M., Jöckel, P., Matthes, S., Nützel, M., Grewe, V., and Sausen, R.: COVID–19 induced lower-tropospheric ozone changes, Environmental Research Letters, 16, 064 005, 2021.

Myhre, G., D.Shindell, Bréon, F.-M., Collins, W., Fuglestvedt, J., Huang, J., Koch, D., Lamarque, J.-F., Lee, D., Mendoza, B., Nakajima, T., Robock, A., Stephens, G., Takemura, T., and Zhang, H.: IPCC AR5, WG1, Chapter 8: Anthropogenic and Natural Radiative Forcing, https://archive.ipcc.ch/pdf/assessment-report/ar5/wg1/WG1AR5_Chapter08_FINAL.pdf, 2013.

Neubauer, D., Ferrachat, S., Siegenthaler-Le Drian, C., Stier, P., Partridge, D. G., Tegen, I., Bey, I., Stanelle, T., Kokkola, H., and Lohmann, U.: The global aerosol–climate model ECHAM6.3–HAM2.3 – Part 2: Cloud evaluation, aerosol radiative forcing, and climate sensitivity, Geoscientific Model Development, 12, 3609–3639, https://doi.org/10.5194/gmd-12-3609-2019, 2019.

Nordeng, T. E.: Exploring the uncertainties in the aviation soot–cirrus effect, ECMWF Tech. Memo., No. 206, 1994.

Petetin, H., Bowdalo, D., Soret, A., Guevara, M., Jorba, O., Serradell, K., and Pérez García-Pando, C.: Meteorology-normalized impact of the COVID–19 lockdown upon NO_2 pollution in Spain, Atmospheric Chemistry and Physics, 20, 11 119–11 141, https://doi.org/10.5194/acp-20-11119-2020, 2020.

Petters, M. and Kreidenweis, S.: A single parameter representation of hygroscopic growth and cloud condensation nucleus activity, Atmospheric Chemistry and Physics, 7, 1961–1971, 2007.

Phillips, V. T., Demott, P. J., Andronache, C., Pratt, K. A., Prather, K. A., Subramanian, R., and Twohy, C.: Improvements to an empirical parameterization of heterogeneous ice nucleation and its comparison with observations, Journal of the Atmospheric Sciences, 70, 378–409, 2013.

Platnick, S., Durkee, P. A., Nielsen, K., Taylor, J. P., Tsay, S.-C., King, M. D., Ferek, R. J., Hobbs, P. V., and Rottman, J. W.: The Role of Background Cloud Microphysics in the Radiative Formation of Ship Tracks, Journal of the Atmospheric Sciences, 57, 2607–2624, https://doi.org/10.1175/1520-0469(2000)057<2607:TROBCM>2.0.CO;2, publisher: American Meteorological Society Section: Journal of the Atmospheric Sciences, 2000.

Pozzer, A., Reifenberg, S. F., Kumar, V., Franco, B., Kohl, M., Taraborrelli, D., Gromov, S., Ehrhart, S., Jöckel, P., Sander, R., Fall, V., Rosanka, S., Karydis, V., Akritidis, D., Emmerichs, T., Crippa, M., Guizzardi, D., Kaiser, J. W., Clarisse, L., Kiendler-Scharr, A., Tost, H., and Tsimpidi, A.: Simulation of organics in the atmosphere: evaluation of EMACv2.54 with the Mainz Organic Mechanism (MOM) coupled to the ORACLE (v1.0) submodel, Geoscientific Model Development, 15, 2673–2710, https://doi.org/10.5194/gmd-15-2673-2022, 2022.

Pringle, K. J., Tost, H., Message, S., Steil, B., Giannadaki, D., Nenes, A., Fountoukis, C., Stier, P., Vignati, E., and Lelieveld, J.: Description and evaluation of GMXe: a new aerosol submodel for global simulations (v1), Geoscientific Model Development, 3, 391–412, https://doi.org/10.5194/gmd-3-391-2010, 2010.

Pruppacher, H. R. and Klett, J. D.: Microphysics of Clouds and Precipitation, 1997.

Quaas, J., Gryspeerdt, E., Vautard, R., and Boucher, O.: Climate impact of aircraft-induced cirrus assessed from satellite observations before and during COVID–19, Environmental Research Letters, 16, 064 051, 2021.

Righi, M., Hendricks, J., and Beer, C. G.: Exploring the uncertainties in the aviation soot–cirrus effect, Atmospheric Chemistry and Physics Discussions, 2021, 1–31, https://doi.org/10.5194/acp-2021-329, 2021.

Roeckner, E., Bäuml, G., Bonaventura, L., Brokopf, R., Esch, M., Giorgetta, M., Hagemann, S., Kirchner, I., Kornblueh, L., Manzini, E., et al.: The atmospheric general circulation model ECHAM 5. PART I: Model description, 2003.

Roeckner, E., Brokopf, R., Esch, M., Giorgetta, M., Hagemann, S., Kornblueh, L., Manzini, E., Schlese, U., and Schulzweida, U.: Sensitivity of simulated climate to horizontal and vertical resolution in the ECHAM5 atmosphere model, Journal of Climate, 19, 3771–3791, 2006.

Schumann, U., Baumann, R., Baumgardner, D., Bedka, S. T., Duda, D. P., Freudenthaler, V., Gayet, J.-F., Heymsfield, A. J., Minnis, P., Quante, M., et al.: Properties of individual contrails: a compilation of observations and some comparisons, Atmospheric Chemistry and Physics, 17, 403–438, 2017.

Schumann, U., Bugliaro, L., Dörnbrack, A., Baumann, R., and Voigt, C.: Aviation Contrail Cirrus and Radiative Forcing Over Europe During 6 Months of COVID–19, Geophysical Research Letters, 48, e2021GL092 771, 2021a.

Schumann, U., Poll, I., Teoh, R., Koelle, R., Spinielli, E., Molloy, J., Koudis, G. S., Baumann, R., Bugliaro, L., Stettler, M., and Voigt, C.: Air traffic and contrail changes over Europe during COVID–19: a model study, Atmospheric Chemistry and Physics, 21, 7429–7450, https://doi.org/10.5194/acp-21-7429-2021, 2021b.

Seinfeld, J. and Pandis, S.: Atmospheric Chemistry and Physics. 1997, New York, 2008.

Shindell, D. T., Lamarque, J.-F., Schulz, M., Flanner, M., Jiao, C., Chin, M., Young, P. J., Lee, Y. H., Rotstayn, L., Mahowald, N., Milly, G., Faluvegi, G., Balkanski, Y., Collins, W. J., Conley, A. J., Dalsoren, S., Easter, R., Ghan, S., Horowitz, L., Liu, X., Myhre, G., Nagashima, T., Naik, V., Rumbold, S. T., Skeie, R., Sudo, K., Szopa, S., Takemura, T., Voulgarakis, A., Yoon, J.-H., and Lo, F.: Radiative forcing in the ACCMIP historical and future climate simulations, Atmospheric Chemistry and Physics, 13, 2939–2974, https://doi.org/10.5194/acp-13-2939-2013, 2013.

Sicard, P., De Marco, A., Agathokleous, E., Feng, Z., Xu, X., Paoletti, E., Rodriguez, J. J. D., and Calatayud, V.: Amplified ozone pollution in cities during the COVID–19 lockdown, Science of The Total Environment, 735, 139 542, https://doi.org/10.1016/j.scitotenv.2020.139542, 2020.

Steinbrecht, W., Kubistin, D., Plass-Dülmer, C., Davies, J., Tarasick, D. W., Gathen, P. v. d., Deckelmann, H., Jepsen, N., Kivi, R., Lyall, N., Palm, M., Notholt, J., Kois, B., Oelsner, P., Allaart, M., Piters, A., Gill, M., Van Malderen, R., Delcloo, A. W., Sussmann, R., Mahieu, E., Servais, C., Romanens, G., Stübi, R., Ancellet, G., Godin-Beekmann, S., Yamanouchi, S., Strong, K., Johnson, B., Cullis, P., Petropavlovskikh, I., Hannigan, J. W., Hernandez, J.-L., Rodriguez, A. D., Nakano, T., Chouza, F., Leblanc, T., Torres, C., Garcia, O., Röhling, A. N., Schneider, M., Blumenstock, T., Tully, M., Paton-Walsh, C., Jones, N., Querel, R., Strahan, S., Stauffer, R. M., Thompson, A. M., Inness, A., Engelen, R., Chang, K.-L., and Cooper, O. R.: COVID–19 Crisis Reduces Free Tropospheric Ozone across the Northern Hemisphere, Geophysical Research Letters, n/a, e2020GL091 987, https://doi.org/10.1029/2020GL091987, e2020GL091987 2020GL091987, 2021.

Sundqvist, H., Berge, E., and Kristjánsson, J. E.: Condensation and cloud parameterization studies with a mesoscale numerical weather prediction model, Monthly Weather Review, 117, 1641–1657, 1989.

Tiedtke, M.: A Comprehensive Mass Flux Scheme for Cumulus Parameterization in Large-Scale Models, Monthly Weather Review, 117, 1779–1800, https://doi.org/10.1175/1520-0493(1989)117<1779:ACMFSF>2.0.CO;2, publisher: American Meteorological Society Section: Monthly Weather Review, 1989.

Tobías, A., Carnerero, C., Reche, C., Massagué, J., Via, M., Minguillón, M. C., Auey, A., and Querol, X.: Changes in air quality during the lockdown in Barcelona (Spain) one month into the SARS–CoV–2 epidemic, Science of The Total Environment, 726, 138 540, https://doi.org/10.1016/j.scitotenv.2020.138540, 2020.

Tost, H., Jöckel, P., and Lelieveld, J.: Influence of different convection parameterisations in a GCM, Atmospheric Chemistry and Physics, 6, 5475–5493, https://doi.org/10.5194/acp-6-5475-2006, 2006.

Tsimpidi, A. P., Karydis, V. A., Pozzer, A., Pandis, S. N., and Lelieveld, J.: ORACLE (v1.0): module to simulate the organic aerosol composition and evolution in the atmosphere, Geoscientific Model Development, 7, 3153–3172, https://doi.org/10.5194/gmd-7-3153-2014, 2014.

Twomey, S.: The nuclei of natural cloud formation part II: The supersaturation in natural clouds and the variation of cloud droplet concentration, Geofisica pura e applicata, 43, 243–249, https://doi.org/10.1007/BF01993560, 1959.

Urbanek, B., Groß, S., Wirth, M., Rolf, C., Krämer, M., and Voigt, C.: High depolarization ratios of naturally occurring cirrus clouds near air traffic regions over Europe, Geophysical research letters, 45, 13–166, 2018.

Van Heerwaarden, C. C., Mol, W. B., Veerman, M. A., Benedict, I., Heusinkveld, B. G., Knap, W. H., Kazadzis, S., Kouremeti, N., and Fiedler, S.: Record high solar irradiance in Western Europe during first COVID–19 lockdown largely due to unusual weather, Communications Earth & Environment, 2, 1–7, 2021.

Venter, Z. S., Aunan, K., Chowdhury, S., and Lelieveld, J.: COVID–19 lockdowns cause global air pollution declines, Proceedings of the National Academy of Sciences, 117, 18 984–18 990, https://doi.org/10.1073/pnas.2006853117, 2020.

Voigt, C., Schumann, U., Minikin, A., Abdelmonem, A., Afchine, A., Borrmann, S., Boettcher, M., Buchholz, B., Bugliaro, L., Costa, A., et al.: ML–CIRRUS: The airborne experiment on natural cirrus and contrail cirrus with the high-altitude long-range research aircraft HALO, Bulletin of the American Meteorological Society, 98, 271–288, 2017.

Voigt, C., Lelieveld, J., Schlager, H., Schneider, J., Curtius, J., Meerkötter, R., Sauer, D., Bugliaro, L., Bohn, B., Crowley, J. N., Erbertseder, T., Groß, S., Hahn, V., Li, Q., Mertens, M., Pöhlker, M., Pozzer, A., Schumann, U., Tomsche, L., Williams, J., Zahn, A., Andreae, M., Borrmann, S., Bräuer, T., Dörich, R., Dörnbrack, A., Edtbauer, A., Ernle, L., Fischer, H., Giez, A., Granzin, M., Grewe, V., Harder, H., Heinritzi, M., Holanda, B., Jöckel, P., Kaiser, K., Krüger, O., Lucke, J., Marsing, A., Martin, A., Matthes, S., Pöhlker, C., Pöschl, U., Reifenberg, S., Ringsdorf, A., Scheibe, M., Tadic, I., Zauner-Wieczorek, M., Henke, R., and Rapp, M.: Cleaner sky during the Covid-19 confinement, Bulletin of the American Meteorological Society, submitted, 2021.

Xu, L. and Penner, J. E.: Global simulations of nitrate and ammonium aerosols and their radiative effects, Atmospheric Chemistry and Physics, 12, 9479–9504, https://doi.org/10.5194/acp-12-9479-2012, 2012.

Yoon, J., Chang, D., Lelieveld, J., Pozzer, A., Kim, J., and Yum, S.: Empirical evidence of a positive climate forcing of aerosols at elevated albedo, Atmospheric Research, 229, 269–279, 2019.

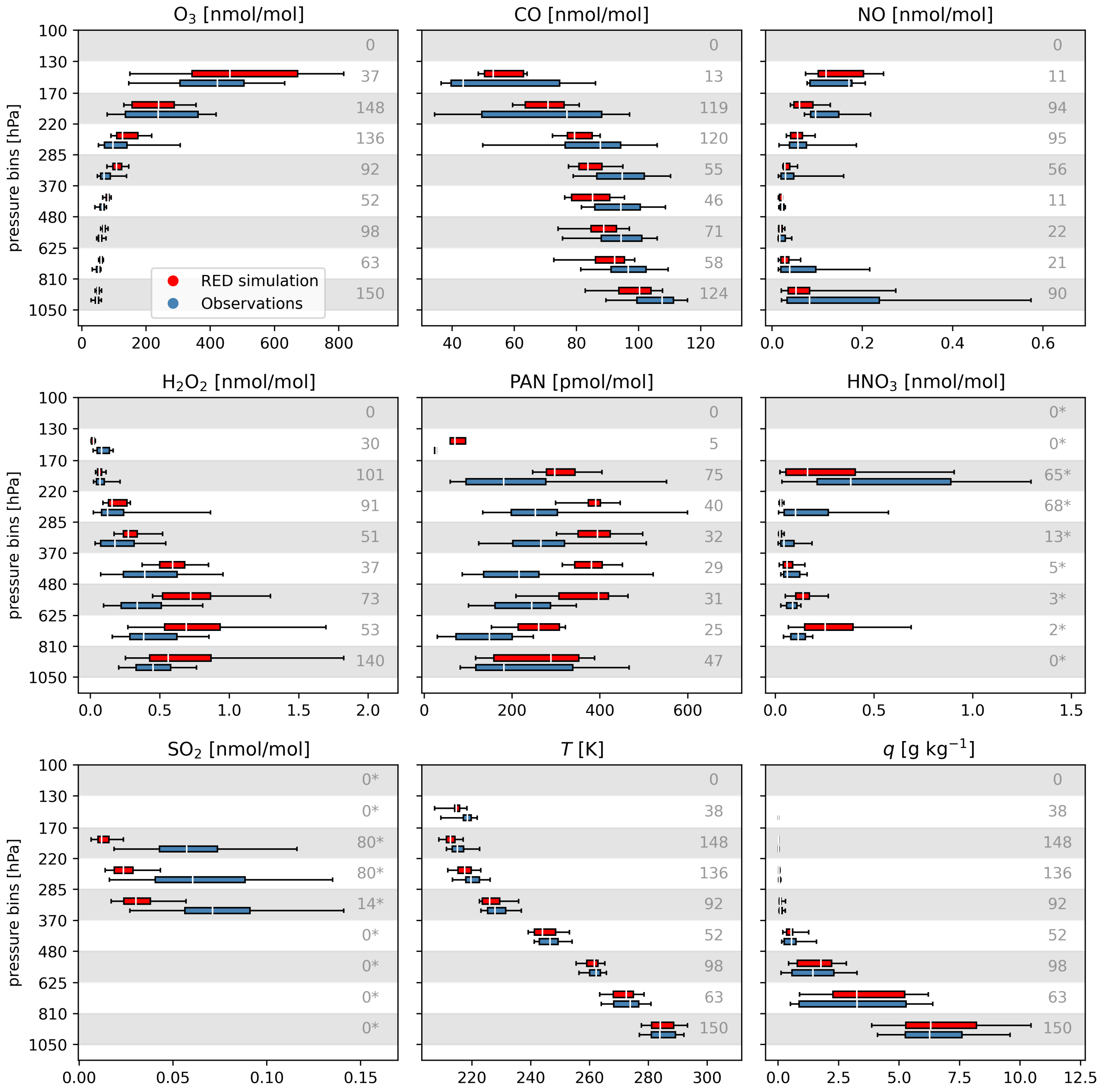

Figure 2. Vertical distribution of simulated (red, ~~"MOD"~~simulation RED) and observed (blue~~, "OBS"~~) tracer mixing ratios and two meteorological variables (T and q), represented by box–whisker plots for pressure bins. The white line marks the median, the box corresponds to lower and upper quartiles, the whiskers represent the 5–95 percentile. The grey numbers on the right indicate the sample size (number of observed and interpolated simulated data points) for each pressure bin. Simulated values are from the RED simulation, i.e. with reduced emissions and no aerosol–cloud interactions. For HNO$_3$ and SO$_2$ (measured onboard of the Falcon aircraft, grey number marked with asterisks) the domain average of the model results over Europe at the corresponding altitude were used, not the values sampled online on the flight track.

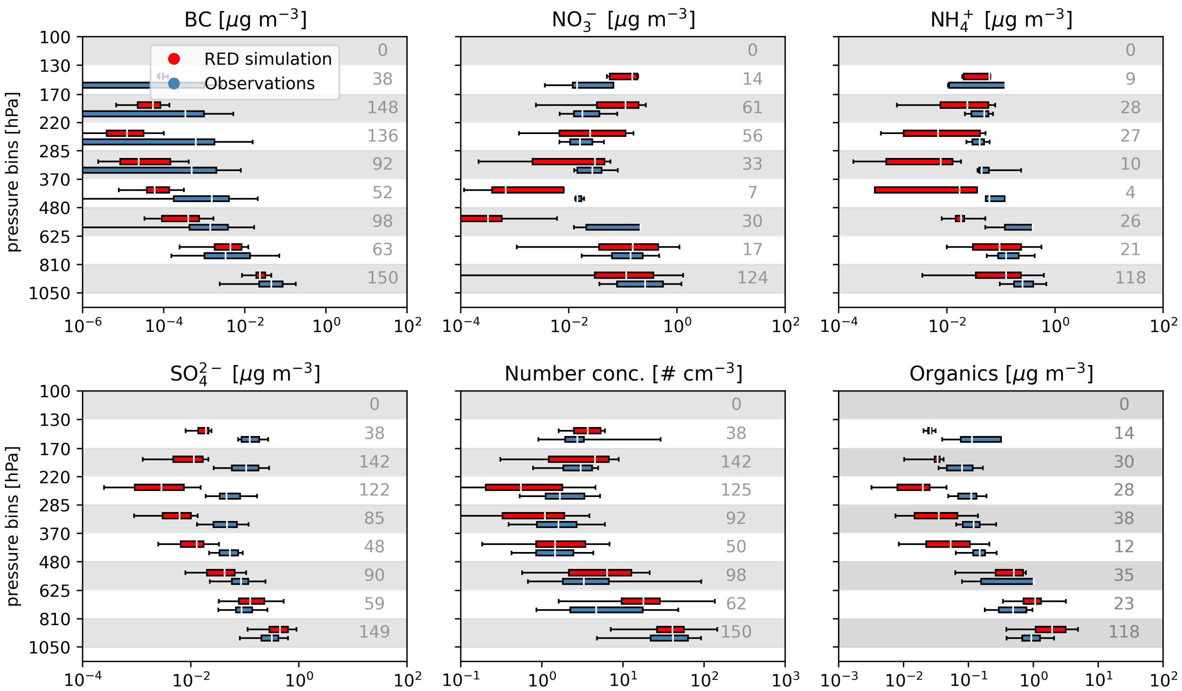

Figure 3. As Fig. 2, but for aerosols. Please note the logarithmic scale in the x-axis.

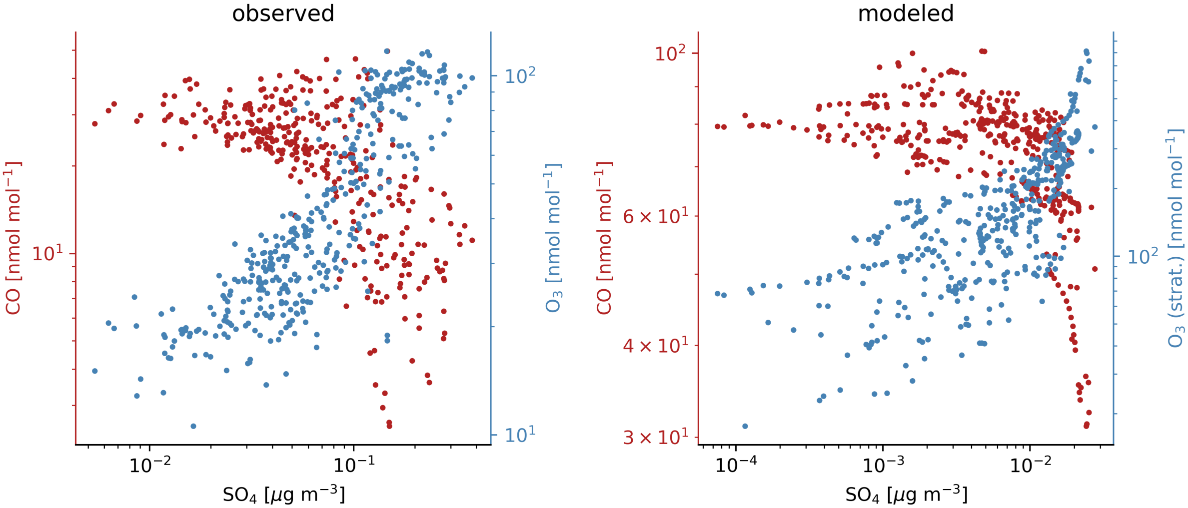

Figure 4. Scatter plot of co-located SO$_4$~~and~~ , CO (red) ~~respective~~ and O$_3$ (blue) abundance between 350 and 150 hPa from observations (left) and the RED simulation (right).

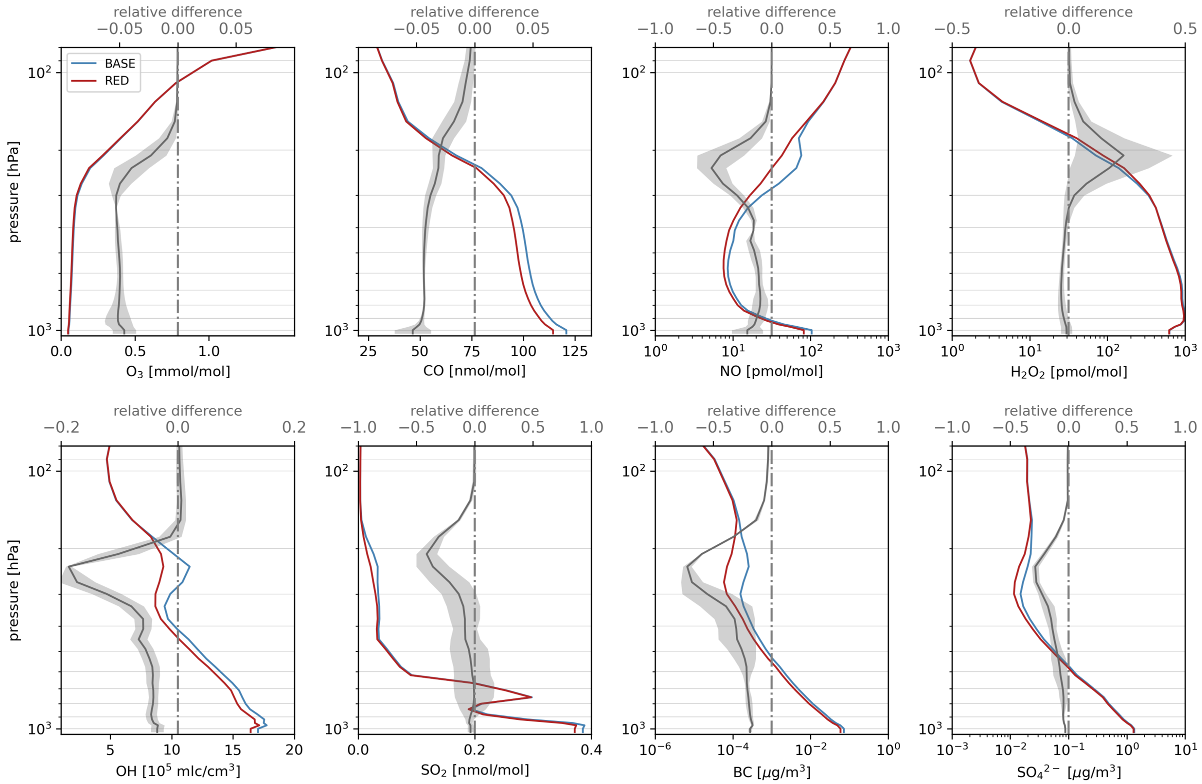

Figure 5. Vertical profiles from ~~STD~~ BASE and RED simulations and their relative difference ((RED−~~STD~~BASE)/~~STD~~BASE). The grey area represents one standard deviation of the spatial-temporal mean (grey line). Please note the different scales for the relative differences.

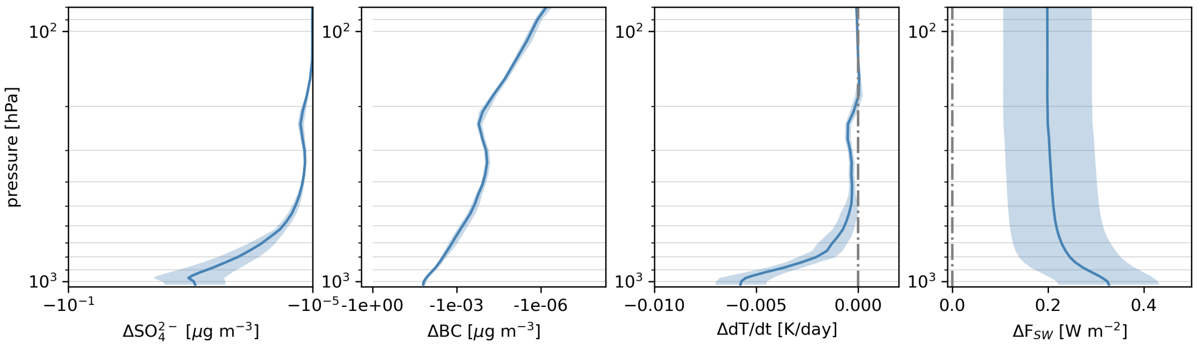

Figure 6. Vertical profiles of the difference of monthly mean sulfate mass concentration (SO_4^{2-}), black carbon mass concentration (BC), heating rate ($\mathrm{d}T/\mathrm{d}t$) and the net shortwave flux (F_{SW}) between the reduced emission scenario RED and the standard emission scenario ~~STD~~BASE. shortwave flux and shortwave heating are derived under clear sky conditions. The shading indicates one standard deviation of the monthly mean difference. Note the logarithmic horizontal axis for the two plots on the left.

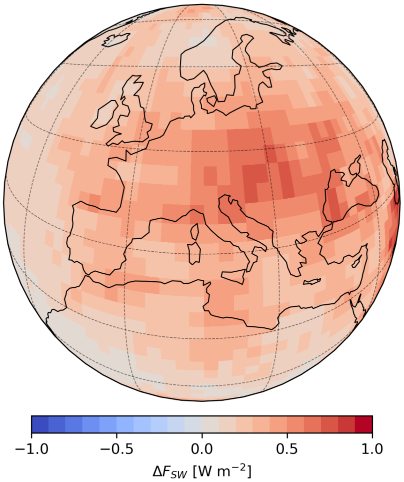

Figure 7. Difference of monthly mean clear sky shortwave radiation (May 2020) at the surface between RED and ~~STD~~ BASE simulation. Positive (red) values indicate more incoming radiation at the surface due to less absorption and backscattering in the "lockdown" atmosphere than in the ~~business as usual~~ baseline scenario. Note that we used a common reduction factor for emissions from countries outside Europe.

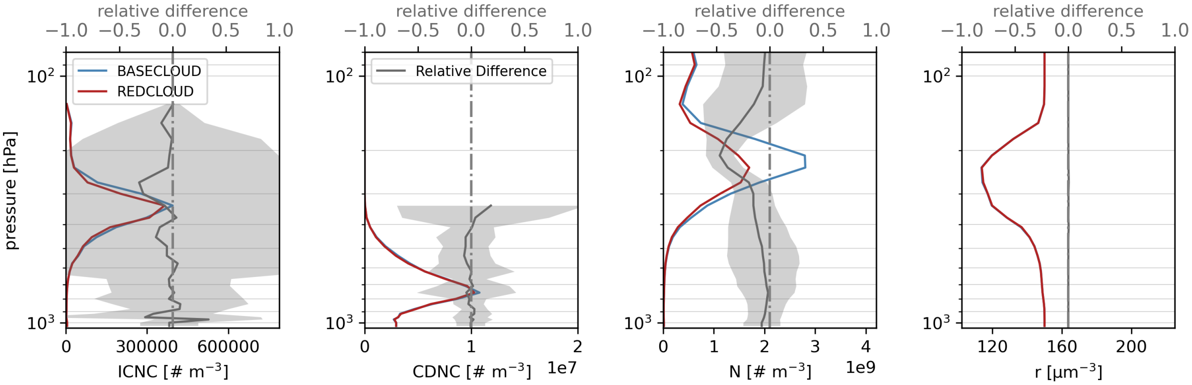

Figure 8. Vertical profiles of the monthly mean ice crystal number concentration (ICNC), cloud droplet number concentration (CDNC), aerosol number concentration (N) and ice crystal effective radius (r) of the reduced emission scenario REDCLOUD (red) and the standard emission scenario ~~STDCLOUD~~ BASECLOUD (blue) and their relative difference (grey line) for May 2020 over Europe. The grey area denote the spatial and temporal standard deviation of the relative difference.